Journal of Inorganic and Organometallic Polymers and Materials
https://doi.org/10.1007/s10904-017-0740-4

A Computational Study of the Adsorptive Removal of H_2S by MOF-199

Hong-Yan Zhang[1] · Zhen-Rong Zhang[2] · Chao Yang[1] · Li-Xia Ling[1] · Bao-Jun Wang[1] · Hui-Ling Fan[1]

Received: 9 September 2017 / Accepted: 11 November 2017

Abstract
Metal–organic framework material MOF-199 is a new type of adsorption material for removal toxic H_2S. In this work, the effects of temperature and pressure on the performance of H_2S adsorption in MOF-199 were studied by using the grand canonical Monte Carlo (GCMC) simulation; the interaction mechanism between framework atoms of MOF-199 and guest H_2S molecules were further discussed through density functional theory (DFT) calculations. It is found that the MOF-199 adsorption capacity towards H_2S decreases with increasing temperature and increases with increasing pressure. At low pressures, the frameworks containing the binding sites of copper dimers and trimesic acid are the main factor affecting the adsorption performance of MOF-199. While at high pressures, the free volume of MOF-199 contributes to the adsorption capacity as well. The adsorptive interactions between H_2S and the organic ligand are weak (>-14.469 kJ/mol). When H_2S adsorption on the Cu–Cu bridge, the binding energies of the modes where hydrogen is put inward of the copper dimer are generally smaller than that where hydrogen is outward, whereas the adsorption on the top of copper ion shows the smallest BEs value (<-50 kJ/mol) due to its tendency of forming a saturated six-coordinated configuration.

Keywords Adsorption · MOF-199 · H_2S · GCMC simulation · DFT calculation

1 Introduction

All forms of fossil fuels generally contain different forms of sulfur as contaminants. Large amounts of hydrogen sulfide are released during the utilization of coal, petroleum and natural gas [1–3], which results in pipeline and building corrosions as well as catalyst pollution [4, 5]. Moreover, hydrogen sulfide is toxic to human health. Therefore, the removal the H_2S from industrial gas stream has become a near mandatory step.

Currently, various H_2S removal technics have been developed, among them, adsorption desulfurization shows the best potential with the advantages of simple operation, less by-products, low energy consumption and easy regeneration [6, 7]. However, selecting appropriate adsorbent plays a decisive role in the desulfurization process [8]. Activated carbon [9, 10], zeolites [11] and porous silicon [12] have been extensively investigated for desulfurization. In the past few years, metal–organic frameworks (MOFs) have attracted considerable attentions due to its prominent advantage of large surface area, adjustable pore structure and modifiable surfaces [13–15]. Thus far, MOFs have showed predominant adsorption performance on H_2S removal, for example, per gram, M-COP-27 can absorb about 10 mmol H_2S [16]. But the diversity of MOFs makes it difficult to properly select an excellent MOF for H_2S removal by only experimental method.

In recent years, the theoretical calculations by computational chemistry method have been widely used as it can be used to quickly predict material performance and explore the microscopic mechanism under MOFs adsorption. Yang Liu et al. [17] studied the effect of functionalized linkers on CO_2 binding in ZIFs with DFT calculations. It proposed that chlorine group of ZIF-69 and nitro group of ZIF-78 could lead to enhanced acidity for the hydrogen atoms on linker and form weak hydrogen bond interactions with the oxygen atoms of CO_2, which has positive effects to enhance the binding capacity of CO_2. Wei Mu et al. [18] demonstrated that MOFs doped with alkali metals can greatly enhance

✉ Hui-Ling Fan
fanhuiling@tyut.edu.cn

[1] State Key Laboratory of Coal Science and Technology, Co-founded by Shanxi Province and the Ministry of Science and Technology, Institute for Chemical Engineering of Coal, Taiyuan University of Technology, West Yingze Street Number 79, Taiyuan 030024, China

[2] Institute of Applied Chemical, Taiyuan, Shanxi, China

Published online: 16 November 2017

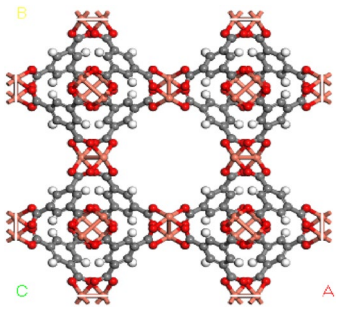

Fig. 1 Topological structure of MOF-199

the adsorption selectivity of CO_2/CH_4 mixture by means of GCMC simulation and DFT calculation.

The high-density and strong adsorption sites on MOF-199 endow it excellent adsorption performance [19]. Our previous experimental works have found that the adsorption capacity of H_2S on MOF-199 was larger than IRMOF-3, IRMOF-8, MOF-74(Zn) and MIL-101 [20–22]. In this work, the effect of external factors and internal mechanism on adsorption of H_2S by MOF-199 were further studied by theoretical calculation, providing us with a better understanding for the dominated factors in MOF-199 gas adsorption.

In the present study, the effect of temperature and pressure on the performance of H_2S adsorption on MOF-199 was studied using the grand canonical Monte Carlo (GCMC) simulation. Meanwhile, the contribution of the fragments of MOF-199 to the adsorption of H_2S were investigated using density functional theory (DFT) calculations.

2 Theoretical Approaches

2.1 Grand Canonical Monte Carlo Method

2.1.1 The Structure of MOF-199

The framework structure of MOF-199 is constructed from its experimental single-crystal X-ray diffraction (XRD) data. The crystal structure is showed in Fig. 1. MOF-199 is assembled from a copper dimer coordinated with four trimesic acid ligands forming 4-vane paddle-wheel units, as shown in Fig. 2. These structural units are connected with each other and form the "cage-channel" structure of MOF-199, whose channel presents a three-dimensional square-shaped with size of 9 × 9 Å and the approximately octahedral pore cages, are 5 Å in size [23–25].

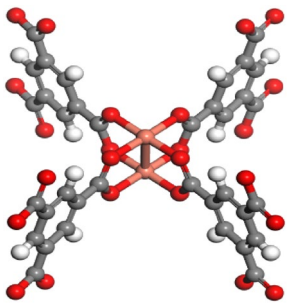

Fig. 2 4-Vane paddlewheel units of MOF-199 (the pink is Cu, the red is O, the white is H, and the gray is C). (Color figure online)

Table 1 The force field parameters and charges of H_2S molecule

Atom	σ (Å)	ε/k_B (K)	Change (e)
H	0.98	3.9	0.124
S	3.72	250.0	−0.248

Table 2 The potential parameters of MOF-199

Atom	σ (Å)	ε/k_B (K)
O	2.96[a]	73.98[b]
$C_{carboxyl}$	3.75[a]	44.91[b]
$C_{benzene}$	3.55[a]	35.23[a]
H	2.42[a]	15.10[a]
Cu	3.11[c]	2.52[c]

[a]OPLS-AA force field developed by Jorgensen et al. [29]

[b]Force field developed by Chongli Zhong et al. [30]

[c]UFF force field [31]

2.1.2 Force Fields and Atomic Charge

The H_2S molecule is described by a three-site model, and the atomic partial charges on each atom are well-distributed. In this work, the parameters of the H_2S molecular refer to the calculation results from Nath [26], in which the H–S bond length is 1.365 Å, H–S–H angle is 91.5 degrees, and the potential parameters are taken from the NERD force field. The force field parameters and charges of H_2S molecule are shown in Table 1.

Potential parameters for the atoms in the framework of MOF-199 are derived from reference [27] as shown in Table 2. Furthermore, the charges of each atom in MOF-199 is calculated based on GAUSSIAN 03 [28], shown in Fig. 3.

2.1.3 Simulation Techniques

The calculations are performed using the GCMC method with Sorption program in Materials Studio 8 software. The Metropolis method is used in all simulation process. The long-range electrostatic interactions are dealt with the Ewald

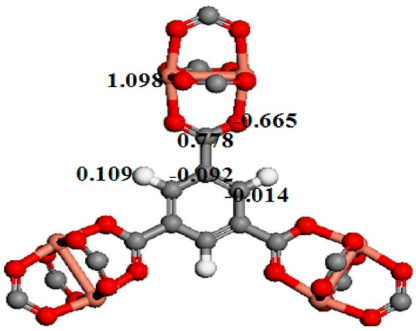

Fig. 3 Atomic charges in clusters of MOF-199

Fig. 4 The CUS of MOF-199

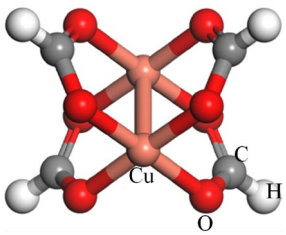

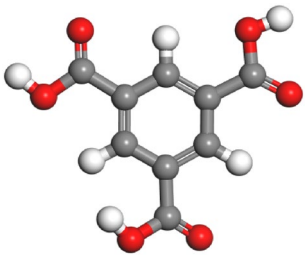

Fig. 5 The organic ligands of MOF-199

Fig. 6 The adsorption configuration used to verify the reliability of the functional (the pink is Cu, the red is O, the white is H, the gray is C, and the yellow is S). (Color figure online)

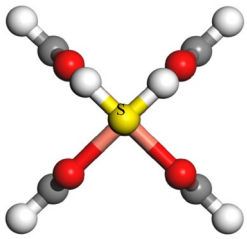

summation technique. A cutoff radius of 12.5 Å is utilized to the LJ interactions. The simulation consists of 5×10^6 steps to guarantee equilibration followed by 5×10^6 steps to obtain the desired thermodynamic properties. The MOF-199 unit cell is geometrically optimized by the Geometry Optimization task in the Forcite template to achieve the minimum energy configuration. In this paper, the adsorptive capacity refers to absolute adsorption capacity. In addition,while the pressure is required to be expressed as fugacity, the selected region of low pressure ranges warrants the assumption that pressure is approximately equal to the fugacity.

2.2 Density Functional Theory Calculation

2.2.1 The Cluster of MOF-199

Coordinatively unsaturated sites (CUS) and organic ligand of MOF-199 are constructed using the Visualizer Material program in Material Studio software. As shown in Figs. 4 and 5, they are obtained by cutting out the periodic structure and introducing protons to saturate the unsaturated atom, keeping the overall charge zero.

2.2.2 Computational Method

The DFT calculations are performed with the Dmol^3 program in Material Studio 8 software. The Perdew–Burke–Ernzerhof (PBE) method based on the generalized gradient approximation (GGA) is used to describe the exchange–correlation interaction. The atom is treated by the All Electron Relativistic method. A double numerical plus (DNP) polarization basis set and a real-space orbital global cutoff of 4.4 Å are applied. Since the standard DFT method is inaccurate in describing long-range electron interactions, this work introduces functional DFT-D2 to compensate. The detailed computational steps are as follows: the adsorbates and MOF cluster are firstly geometrically optimized to obtain a stable configuration, and their respective energies are calculated and expressed as $E(A)$ and $E(B)$. Then, the various orientations adsorption configurations are optimized respectively to obtain the corresponding energy values, expressed as $E(AB)$. The binding energy (BE) between the adsorbates and MOFs is defined as follows: $BE = E(AB) - (E(A) + E(B))$ [17]. A higher absolute value of BE indicates a higher adsorption strength.

2.2.3 Verification the Accuracy of the Methods

It is necessary to verify whether the D2 dispersion correction can get better results. It should be mentioned that the accuracy of the BE obtained by the MO6-L functional calculation is even higher than that obtained at the MP2 level in the MOF systems [32]. Therefore, calculated results by the MO6-L functional are considered as a measurement standard to verify the results from PBE and PBE-D2 functional. The adsorption configuration used to verify the reliability of the DFT functions is shown in Fig. 6. The BEs calculated by MO6-L, PBE and PBE-D2 functionals are − 53.502 kJ/mol, − 41.668 kJ/mol and − 52.206 kJ/mol, respectively. The BE obtained from the PBE-D2 functional is very close to that of the MO6-L functional. Since the MO6-L calculation

requires a larger computational resources than PBE-D2, the PBE-D2 method is used in this work.

3 Results and Discussion

3.1 H_2S Adsorption Over MOF-199 with GCMC Method

3.1.1 Effect of Temperature on Adsorption

The adsorption performance was found to be highly influenced by the temperature. The effect of temperature range of 0–65 °C on H_2S adsorption over MOF-199 were investigated under three pressures (0.1, 0.2, 0.3 Mpa). The results are shown in Fig. 7, adsorption capacity gradually decreased with increasing temperature under the same pressure. At atmospheric pressure, the maximum adsorption capacity at 0 °C (15.1 mmol/g), while the minimum was at 60 °C (2.8 mmol/g). The adsorption capacity was half of the maximum when the temperature was 25 °C. Apparently temperature has a dramatic influence on the adsorption of MOF-199. This is to be expected as thermal motion intensifies with increasing temperature. The increased kinetic energy of H_2S molecules decreased the effectiveness of the adsorptive interactions between H_2S and MOF. Therefore, the residence time of the H_2S molecules on the surface of MOF-199 was shortened, leading to a lower adsorption capacity. This is consistent with experimental results which showed that the adsorption capacity of MOF-74(Ni) for C_3H_6 and C_3H_8 decreased with increasing temperature [33]. It is worth noting that our previous experimental study showed that the breakthrough sulfur capacity of MOF-199 for H_2S removal was only 1.27 mmol/g at 30 °C and normal pressure [20]. Whereas indicated in Fig. 7, the absolute adsorption capacity under the same conditions was 6.6 mmol/g. The tremendous difference in the equilibrium value indicates that MOF-199 has very low utilization in the dynamic tests, and it is necessary to improve the adsorption kinetics of MOF-199.

3.1.2 Effect of Pressure on Adsorption

Figure 8 shows the 25 °C adsorption isotherm of H_2S over MOF-199 with the pressure ranging from 0.001 to 0.9 Mpa. The corresponding differential curve is also presented in the Fig. 8. As expected, the adsorption capacity increased with increasing pressure. When the pressure was lower than 0.2 Mpa, the adsorption capacity increased sharply. As the pressure was further increased beyond 0.3 Mpa, the increase was more incremental. When the pressure was higher than 0.4 Mpa, the adsorption capacity plateaued. With the pressure increased, the probability of H_2S adsorbing onto the surface of MOF-199 increases, which causes an acceleration of gas adsorption and an increase in H_2S concentration on the surface of MOF-199, thus the adsorption capacity increases. However, the limitations of pore volume and surface area of the material finally lead to a dynamic adsorption equilibrium.

3.1.3 Density Distribution of H_2S Adsorption on MOF-199

Figure 9 shows the density distribution of the adsorbed H_2S molecules on MOF-199 at various pressures. When the pressure approached zero, H_2S molecules were adsorbed onto the copper dimers and trimesic acid binding sites of MOF-199. As the pressure was gradually increased, H_2S molecules started to occupy the pores of MOF-199. When pressure was up to 0.9 Mpa, almost all pores in MOFs were filled by the

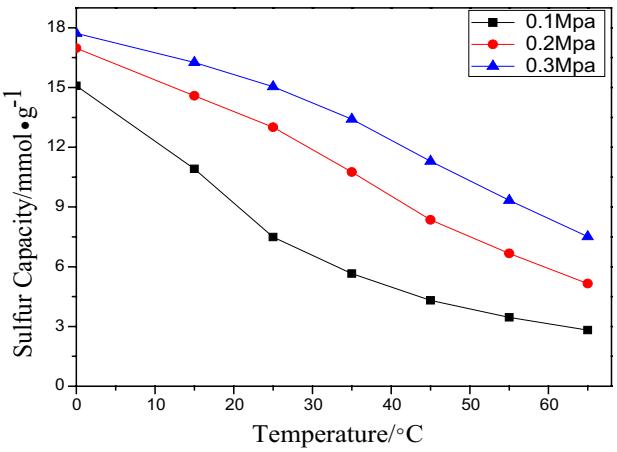

Fig. 7 The sulfur capacity of H_2S adsorption in MOF-199 at different temperature

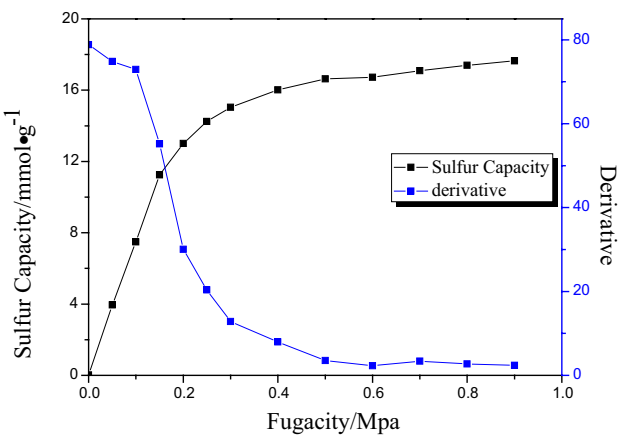

Fig. 8 Adsorption isotherm curve and differential curve of MOF-199 adsorption H_2S

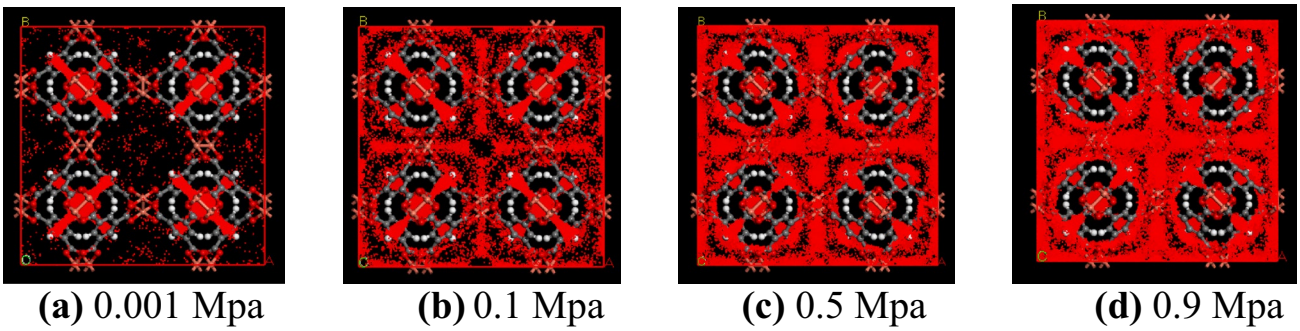

Fig. 9 Density distribution of H_2S molecules adsorption by MOF-199

H_2S guest molecule. The results show that under the lower pressure, H_2S are preferentially adsorbed at the binding sites of MOF-199, while at higher pressures, the free volume of MOF-199 contributes to the adsorption capacity as well. This also indicates that H_2S occupies MOF-199's binding sites more readily than the void space (pores) of MOF-199.

3.2 H_2S Adsorption Over MOF-199 Fragment with DFT Calculation

From the above results, the binding sites of MOF-199 are clearly crucial for H_2S adsorption at low pressure. Therefore, the further investigation of specific interaction mechanisms between the framework atoms of MOF-199 and guest H_2S molecules is of the utmost significance for designing and synthesizing new MOFs with higher H_2S uptake capacity.

The GCMC method has been widely used to investigate the guest molecule adsorptions such as gas uptakes and heats of adsorption in porous materials in various force fields [34, 35]. However, DFT calculation is a quantum chemical method and offers the valuable advantage of revealing the adsorption mechanism [17]. In this section, the mechanism of H_2S adsorption on MOF-199 fragments was studied using DFT calculation.

3.2.1 H_2S Adsorption on Trimesic Acid of MOF-199

Adsorption orientations of H_2S on the organic ligand of MOF-199 are analyzed, as shown in Fig. 10. H_2S molecules were placed vertically (including configuration (a) and configuration (b)) or in the same plane as (including configuration (c) and configuration (d)) the benzene ring of trimesic acid. Adsorption configurations near oxygen atoms were not considered since the oxygen atoms of trimesic acid were bounded with the copper ions in the periodic structure of MOF-199. The optimized structures and BEs are shown in Fig. 10.

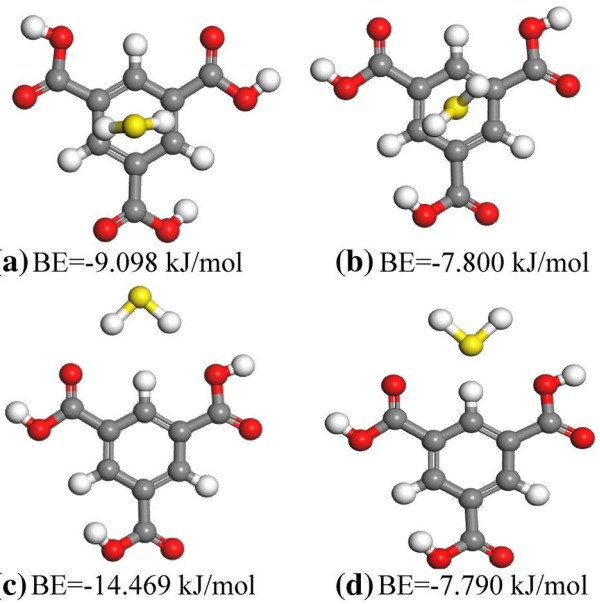

Fig. 10 DFT optimized structures and the corresponding BEs

The BEs of H_2S adsorption on the trimesic acid are from − 14.469 to − 7.790 kJ/mol, which are all in the range of physical adsorption. When the hydrogen sulfide was placed vertically to the ring, the BE of configuration (a) was slightly smaller than that of configuration (b), indicating hydrogen atoms in H_2S are more accessible to the benzene ring than the sulfur atom. When the hydrogen sulfide was placed in the same plane as the benzene ring, the BE of the configuration (c) was significantly smaller than that of the configuration (d) which may be the result of the strong interaction between the two hydrogen atoms of hydrogen sulfide and the two oxygen atoms of the trimesic acid.

3.2.2 H_2S Adsorption on Metal Center of MOF-199

The H_2S adsorption configurations on the copper metal center of MOF-199 are presented, including H_2S on the upper part and the middle of the Cu–Cu bridge, and on the top of copper ion, as shown in Tables 3 and 4.

The optimized structures and BEs of H_2S adsorption in the upper part and the middle of Cu–Cu bridge in Table 3 were calculated and listed in Table 5. The BEs of the eight configurations differ remarkably, range from − 18.269 to 3.774 kJ/mol, but are in the range of physical adsorption. The positive 3.774 kJ/mol indicates that H_2S molecules is barely adsorbed by this configuration. As can be seen from

Table 3 Initial adsorption modes (upper and middle)

Initial models	H-O-V	H-O-P	H-I-V	H-I-P
Upper part	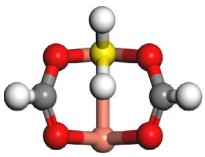	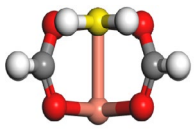	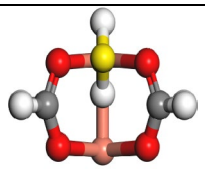	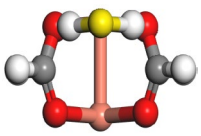
Middle	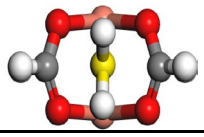	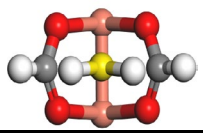	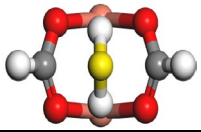	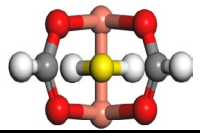

H hydrogen, *O* outward, *I* inward, *V* vertical, *P* parallel

Table 4 Initial adsorption modes (top)

Initial models	Parallel overlap	Parallel cross	Vertical cross	Vertical overlap
Top	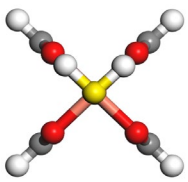	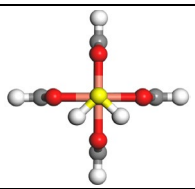	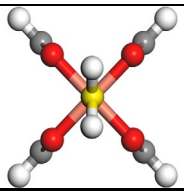	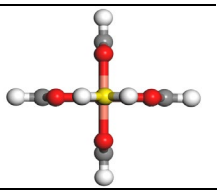

Table 5 Optimized structures and BEs (upper and middle)

Initial models	H-O-V	H-O-P	H-I-V	H-I-P
Stable adsorption configurations (upper part)	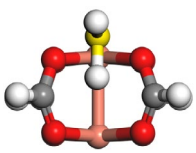	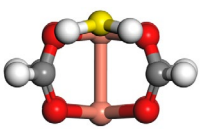	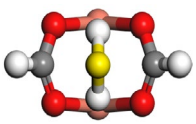	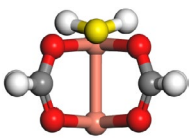
BE（kJ/mol）	−6.818	−7.349	−18.269	−14.229
Stable adsorption configurations (middle)	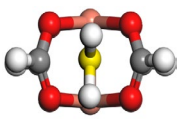	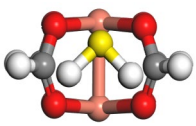	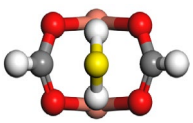	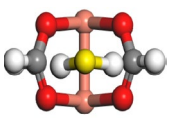
BE（kJ/mol）	3.774	−6.800	−17.872	−2.549

H hydrogen, *O* outward, *I* inward, *V* vertical, *P* parallel

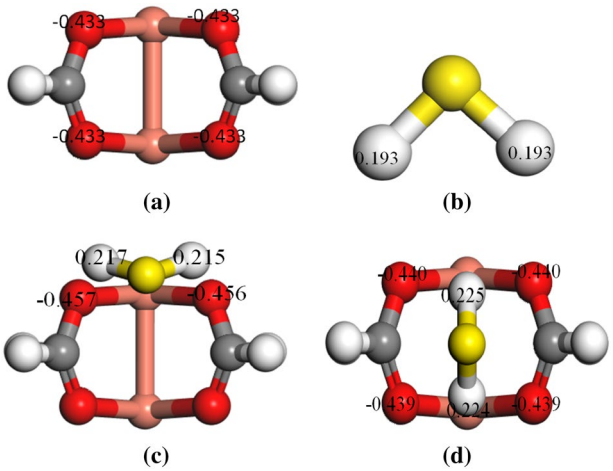

Fig. 11 Mulliken layout analysis. The figure **a** shows the charges of the metal center of MOF-199, **b** is the charges of H_2S molecules, **c** and d are the charges of the stable adsorption configurations

Table 5, the BEs of the modes where hydrogen was put inward of the copper dimer are generally smaller than that of when the hydrogen was placed outward. This might be due to the interaction between the hydrogen atom of H_2S and the oxygen atom of copper metal center. To clarify this assumption, the Mulliken changes of the substrate, H_2S molecule and the optimized structures were also calculated, which is shown in Fig. 11.

The negative charge of the oxygen atom and the positive charge of the hydrogen atom increased as the two atoms approach, illustrating charge transfer occurred between the hydrogen atom and the oxygen atom. Moreover, this also indicates that there exists strong interactions between H and O atoms, which lead to a small BE.

The optimized structures and BEs of the adsorbed H_2S molecules over top the copper ion of M0F-199 are shown in Table 6. The values of BEs are from − 52.206 to − 50.511 kJ/mol, which are in the range of chemical adsorption, indicating that H_2S molecules prefer to adsorb on the top of the copper ion. Actually, the top position is the coordination position of the copper ion. This implies that the interaction originated from the coordination between the lone pair of sulfur and the unsaturated copper center which intends to form a saturated six-coordinated stable configuration. Compared to the weak adsorptive interactions between H_2S and the organic ligand (>− 14.469 kJ/mol), it is suggested that it is the copper metal centers which mainly contributes to H_2S adsorption.

4 Conclusion

In this work, the effects of temperature and pressure on H_2S adsorption over MOF-199 were studied with GCMC method, and the mechanisms of H_2S adsorption on organic ligand and inorganic metal center of MOF-199 were investigated using DFT. The conclusions are summarized as follows:

(1) The MOF-199 adsorption capacity towards H_2S decreases with increasing temperature, and increases with increasing pressure. When the pressure was higher than 0.4 Mpa, the adsorption tended to an equilibrium.
(2) At low pressures, the framework containing the binding sites of copper dimers and trimesic acid is the main factor affecting the adsorption performance of MOF-199. While at high pressures, the free volume of MOF-199 contributes to the adsorption capacity as well.
(3) The adsorptive interactions between H_2S and the organic ligand are weak (>− 14.469 kJ/mol). The configuration with H_2S placed in the same plane as the benzene ring with hydrogen atoms of H_2S close to the oxygen atoms of trimesic acid, is the most stable adsorption configuration for H_2S to adsorb onto the organic ligand.
(4) When H_2S adsorbs onto the Cu–Cu bridge, the BEs of the modes with hydrogen placed inward of the copper dimer are generally smaller than that where hydrogen is outward. The adsorption on the top of copper ion show the smallest BEs value (<− 50 kJ/mol) due to the trend of forming a saturated six-coordinated configuration.

Table 6 Optimized structures and BEs (top)

Initial models	Parallel overlap	Parallel cross	Vertical cross	Vertical overlap
Stable adsorption configurations (top)				
BE（kJ/mol）	–51.738	–50.511	–51.647	–52.206

Acknowledgements Financial supports from National Nature Science Fundamental (21576180) and from the Key Projects of National Natural Science Foundation of China (21736007) are gratefully acknowledged.

References

1. L.P. Chang, Z.Y. Zhang, X.R. Ren, F. Li, K.C. Xie, Energy Fuels **23**, 762 (2009)
2. I. Ahmed, S.H. Jhung, J. Hazard. Mater **301**, 259 (2016)
3. Y. Belmabkhout, N. Heymans, G. De Weireld, A. Sayari, Energy Fuels **25**, 1310 (2011)
4. L. Li, D.L. King, Catal. Today **116**, 537 (2006)
5. L. Hamon, H. Leclerc, A. Ghoufi, L. Oliviero, A. Travert, J.C. Lavalley, T. Devic, C. Serre, G. Férey, J. Phys. Chem. C **115**, 2047 (2011)
6. A. Samokhvalov, B.J. Tatarchuk, Catal. Rev. **52**, 381 (2010)
7. N.A. Khan, Z. Hasan, S.H. Jhung, Adv. Porous Mater. **1**, 91 (2013)
8. Z.P. Chen, L.X. Ling, B.J. Wang, H.L. Fan, J. Shangguan, J. Mi, Appl. Surf. Sci. **387**, 483 (2016)
9. X.X. Wu, V. Schwartz, S.H. Overbury, T.R. Armstrong, Energy Fuels **19**, 1774 (2005)
10. R.H. Shi, Z.R. Zhang, H.L. Fan, T. Zhen, J. Shangguan, J. Mi, Appl. Surf. Sci. **394**, 394 (2017)
11. C. Laborde-Boutet, G. Joly, A. Nicolaos, M. Thomas, P. Magnoux, Ind. Eng. Chem. Res. **45**, 6758 (2006)
12. J.H. Park, L. Gu, G. von Maltzahn, E. Ruoslahti, S.N. Bhatia, M.J. Sailor, Nat. Mater. **8**, 331 (2009)
13. J. Liu, Y. Wang, A.I. Benin, P. Jakubczak, R.R. Willis, M.D. LeVan, Langmuir **26**, 14301 (2010)
14. H.H. Wu, Q.H. Gong, D.H. Olson, J. Li, Chem. Rev. **112**, 836 (2012)
15. D. Farrusseng, S. Aguado, C. Pinel, Angew. Chem. Int. Ed. **48**, 7502 (2009)
16. C. Petit, B. Mendoza, T.J. Bandosz, Chem. Phys. Chem. **11**, 3678 (2010)
17. Y. Liu, J. Liu, M. Chang, C.G. Zheng, J. Phys. Chem. C **116**, 16985 (2012)
18. W. Mu, D.H. Liu, C.L. Zhong, Microporous Mesoporous Mater **143**, 66 (2011)
19. L.M. Wu, J. Xiao, Y. Wu, S.K. Xian, G. Miao, H.H. Wang, Z. Li, Langmuir **30**, 1080 (2014)
20. Y. Li, L.J. Wang, H.L. Fan, J. Shangguan, H. Wang, J. Mi, Energy Fuels **29**, 298 (2014)
21. X.L. Wang, H.L. Fan, Z. Tian, E.Y. He, J. Shangguan, Appl. Surf. Sci. **289**, 107 (2014)
22. C. Zhiping, *Taiyuan University of Technology, Taiyuan* (2016)
23. B. Supronowicz, A. Mavrandonakis, T. Heine, J. Phys. Chem. C **117**, 14570 (2013)
24. K. Schlichte, T. Kratzke, S. Kaskel, Microporous Mesoporous Mater **73**, 81 (2004)
25. L. Hamon, E. Jolimaître, G.D. Pringruber, Ind. Eng. Chem. Res. **49**, 7497 (2010)
26. S.K. Nath, J. Phys. Chem. B **107**, 9498 (2003)
27. Q.Y. Yang, C.L. Zhong, J. Phys. Chem. B **110**, 17776 (2006)
28. M.J. Frisch, G.W. Trucks, H.B. Schlegel, G.E. Scuseria, M.A. Robb, J.R. Cheeseman, J.M. Millam, *Gaussian 09, Revision A. 02* (Gaussian Inc., Wallingford CT, 2003)
29. W.L. Jorgensen, D.S. Maxwell, J. Tirado-Rives, J. Am. Chem. Soc. **118**, 11225 (1996)
30. Q.Y. Yang, C.L. Zhong, Chem. Phys. Chem. **7**, 1417 (2006)
31. A.K. Rappé, C.J. Casewit, K.S. Colwell, W.A. Goddard, W.M. Skid, J. Am. Chem. Soc. **114**, 10024 (1992)
32. L. Grajciar, P. Nachtigall, O. Bludský, M. Rubeš, J. Chem. Theor. Comput. **11**, 230 (2014)
33. J. Liu, Y.F. Wu, F. Xu, J. Xiao, Q.B. Xia, Z. Li, J. Chem. Eng. **67**, 1942 (2016)
34. M.P. Allen, D.J. Tildesley, *Computer Simulations of Liquids* (Clarendon, Oxford, 1987)
35. J. Yu, L.H. Xie, J.R. Li, Y.G. Ma, J.M. Seminario, P.B. Balbuena, Chem. Rev. (2017)